Biosensors and Bioelectronics 126 (2019) 332–338

Contents lists available at ScienceDirect

Biosensors and Bioelectronics

journal homepage: www.elsevier.com/locate/bios

Red light-driven photoelectrochemical biosensing for ultrasensitive and scatheless assay of tumor cells based on hypotoxic $AgInS_2$ nanoparticles

Jing Li, Xiaofeng Lin, Zhiyi Zhang, Wenwen Tu*, Zhihui Dai*

Jiangsu Collaborative Innovation Center of Biomedical Functional Materials and Jiangsu Key Laboratory of Biofunctional Materials, College of Chemistry and Materials Science, Nanjing Normal University, Nanjing 210023, PR China

ARTICLE INFO

Keywords:
Photoelectrochemical biosensing
Scatheless assay
Tumor cells
$AgInS_2$ nanoparticles

ABSTRACT

A novel red light-driven photoelectrochemical (PEC) biosensing platform based on hypotoxic ternary mercaptopropionic acid (MPA)-capped $AgInS_2$ nanoparticles (NPs) with excellent hydrophily and biocompatibility was proposed. $AgInS_2$ NPs as a PEC sensing substrate exhibited high photon-to-current conversion efficiency under red light excitation, generating an intensive photocurrent for enhancing the sensitivity of PEC determination. After the introduction of the amino-terminated sgc8c aptamer onto the interface of $AgInS_2$ NPs, the over-expressed protein tyrosine kinase-7 on the surface of lymphoblast CCRF-CEM cells could be efficiently captured. Using CCRF-CEM cell as a model analyte, an ultrasensitive PEC biosensor for scatheless assay of cells at the applied potential of 0.15 V under a red light excitation of 630 nm was designed based on the significant decline of photocurrent intensity after capturing CCRF-CEM cells. The developed PEC cytosensor demonstrated an excellent cell-capture ability, as well as a wide linear range from 1.5×10^2 to 3.0×10^5 cells/mL and a low detection limit of 16 cells/mL for CCRF-CEM cells. In addition, the resulting assay method verified high selectivity and negligible cytotoxicity for cells assay. This work provided an alternative method for scatheless assay of tumor cells, which would have promising prospect in clinical diagnoses of cancer.

1. Introduction

Photoelectrochemical (PEC) measurement is a newly grown and exuberantly developing bioanalysis technique, which possesses a low background signal and high sensitivity than that of the conventional methods (Hu et al., 2018; Wen and Ju, 2016). In the PEC biosensing, the output photocurrent signals based on the photoelectric conversion characteristics of active materials are vital to the construction of the PEC biosensor for monitoring the biorecognition event (Tu et al., 2018; Zhao et al., 2017, 2015), including enzymes analysis (Fan et al., 2015; Zhao et al., 2017), DNA sensing (Zang et al., 2015), proteins detection (Wang et al., 2018), cells-related assay (Li et al., 2015; Tang et al., 2014) and the determination of other small molecules (Feng et al., 2018). Recently, TiO_2 (Feng et al., 2018; Li et al., 2015; Tang et al., 2014), ZnO (Li et al., 2014) and g-C_3N_4 (Dai et al., 2016; Li et al., 2017) as popular photoelectrochemically active materials have been widely adopted to develop PEC biosensors for improving their detection sensitivity. Nevertheless, the above materials have low light utilization efficiency (Yan et al., 2016) and their wide band gap energy only permits them to be excited by ultraviolet light (Li et al., 2012; Qiu et al., 2018) which may make the biomolecules denatured, leading to the limitation of their application to the biosensing. Therefore, some novel explored materials instead of the above materials are urgent to be applied in the PEC biosensing.

The increasing ternary I−III−VI semiconductor materials have displayed their technical applications from optoelectronics (Gromova et al., 2017; Yarema et al., 2018) to biotechnology (Shen and Wang, 2013; Zhong et al., 2012). These materials possess some apparent advantages for real-life applications: they are composed of low toxicity elements compared with traditional binary materials (CdS, CdTe, HgTe, PbS, PbSe, etc.) (Sandroni et al., 2017; Subramaniam et al., 2012); These materials have a high absorption coefficient from the visible to near-infrared region (Jara et al., 2014); The tuning of the band gap can be implemented by controlling its size (Foda et al., 2014; Kameyama et al., 2018), which enhances the photovoltaic conversion efficiency. As a typical ternary I−III−VI semiconductor material, silver indium sulfide ($AgInS_2$) was reported to have a direct band gap (Shen et al., 2013) and its band gap could be tuned by varying the Ag:In precursor ratio, therefore the emission peak of ternary $AgInS_2$ could move from visible to near-infrared region (Dai et al., 2012; Hong et al., 2012). Due to the mentioned advantages, $AgInS_2$ has been utilized in recently biomedical investigations. For example, the $AgInS_2$/ZnS nanocrystals exhibited

* Correspondence authors.
E-mail addresses: wwt@njnu.edu.cn (W. Tu), daizhihuii@njnu.edu.cn (Z. Dai).

https://doi.org/10.1016/j.bios.2018.09.096
Received 16 July 2018; Received in revised form 16 September 2018; Accepted 29 September 2018
Available online 03 October 2018
0956-5663/

high photoluminescence quantum yields and were used as fluorescent sensing probes for monitoring copper (II) levels in HeLa cells (Xiong et al., 2013). The water-dispersible $AgInS_2$/ZnS quantum dots were employed as biological imaging agents for HeLa cells imaging (Shamirian et al., 2015) owing to their near-infrared (NIR) emission. Besides, $AgInS_2$ has been demonstrated as a sensitizer in solar cells for its high photoelectrical activity (Halder and Bhattacharyya, 2017; Kobosko et al., 2017). Moreover, $AgInS_2$ owns the properties of environment-friendly (Kobosko et al., 2017), high photovoltaic conversion efficiency (Hamanaka et al., 2011) and tunable emission wavelength (Wang et al., 2017). Taking into account of the above merits, $AgInS_2$ could be inferred as an attractive candidate for fabricating PEC biosensor to improve its analytical performance in this work.

What should be noticed is that, there is still none exploration about applying $AgInS_2$ in the construction of PEC sensor up to now. Herein, ternary MPA-capped $AgInS_2$ nanoparticles (NPs) with excellent hydrophily and biocompatibility were prepared and used as PEC biosensing substrate material. The ternary $AgInS_2$ NPs exhibited a steady and intensive photocurrent response, which effectively improved the sensitivity of the PEC detection. Recently, several researches suggested that the overexpressed protein tyrosine kinase-7 on the surface of lymphoblast CCRF-CEM cells could be efficiently captured by the sgc8c aptamer which retained unchanged hairpin-like shape after recognition (Cao et al., 2017; Gai et al., 2016; Pang et al., 2018). The sgc8c aptamer is a hairpin-shaped DNA, which is selected by a cell-SELEX (systematic evolution of ligands by exponential enrichment) strategy (Shangguan et al., 2007). Therefore, using CCRF-CEM cell as a model analyte, we designed an ultrasensitive PEC biosensor for scatheless assay of cells under a red light excitation of 630 nm (Scheme 1). The sgc8c aptamer was covalently immobilized on the surface of the MPA-capped $AgInS_2$ NPs for the capture of CCRF-CEM cells. When the CCRF-CEM cells were specifically captured by the sgc8c aptamer, the photoinduced electron transfer would be remarkably hampered due to that the steric hindrance of the target cells could cause a significant decline of photocurrent intensity. Moreover, the surface of CCRF-CEM cells possessed hydrophobicity which blocked the hydrophilic electron donor to the surface of $AgInS_2$ NPs, leading to the further descending of the PEC response. The dramatic difference of photocurrent intensity before and after capturing CCRF-CEM cells beneficially provided ultrahigh sensitivity for PEC detection of CCRF-CEM cells. The proposed ultrasensitive assay method also displayed good selectivity and hypotoxicity for scatheless assay of cells, which would open up an avenue for early diagnoses of leukemia.

2. Experimental section

2.1. Materials and reagents

Tris (hydroxymethyl) aminomethane (Tris) and mercaptopropionic acid (MPA, 97%) were purchased from Alfa Aesar. Ethylene glycol, silver nitrate ($AgNO_3$) and ascorbic acid (AA) were purchased from Sinopharm Chemical Reagent Co. Ltd. 1-Ethyl-3-[(3-dimethylamino)-propyl)] carbodiimide (EDC), indium (III) acetate (99.99%), bovine serum albumin (BSA) and N-hydroxysuccinimide (NHS) were obtained from Sigma-Aldrich. The following sgc8c aptamer was synthesized by Shanghai Sangon Biotechnology Co. Ltd. (5′-ATC TAA CTG CTG CGC CGC CGG GAA AAT ACT GTA CGG TTA GAT TTT TTT TTT-$(CH_2)_6$-NH_2–3′; 5′-Cy3-ATC TAA CTG CTG CGC CGC CGG GAA AAT ACT GTA CGG TTA GA-3′). All of the other reagents were analytical reagent grade. Indium tin oxide (ITO) glass obtained from Jintan Kondrk Photoelectric Science & Technology Co. Ltd. was used as work electrode. Ultrapure water used in all process was purified by a Millipore water purification system (≥ 18 MΩ cm, Millipore SAS Corporation, France). The washing solution was 0.01 M Tris-HCl buffer saline (pH 7.4) containing 0.1 M sodium chloride and 0.05 M potassium chloride.

2.2. Apparatus

Transmission electron microscope (TEM) image was characterized by using a Hitachi H-7650 type transmission electron microscope at an accelerating voltage of 80 kV (Hitachi, Japan). X-ray powder diffraction (XRD) pattern was obtained by a D/max 2500 VL/PC diffractometer (Japan) equipped with graphite monochromatized Cu Ka radiation. Ultraviolet-visible (UV–vis) absorption and photoluminescence (PL) spectra measurements were severally executed on a Cary 60 spectrophotometer (Agilent, USA) and a RF-5301PC fluorescence spectrometer (Shimadzu, Japan). Fourier transform infrared (FTIR) spectrum was acquired on Tensor 27 (Bruker, Germany). The PEC measurements were carried out on a Zahner PEC workstation (Zahner, Germany). Electrochemical impedance spectroscopy (EIS) was implemented on an Autolab PGSTAT302N electrochemical workstation with an external voltage of 10 mV and the frequency range from 0.1 Hz to 100 kHz. The

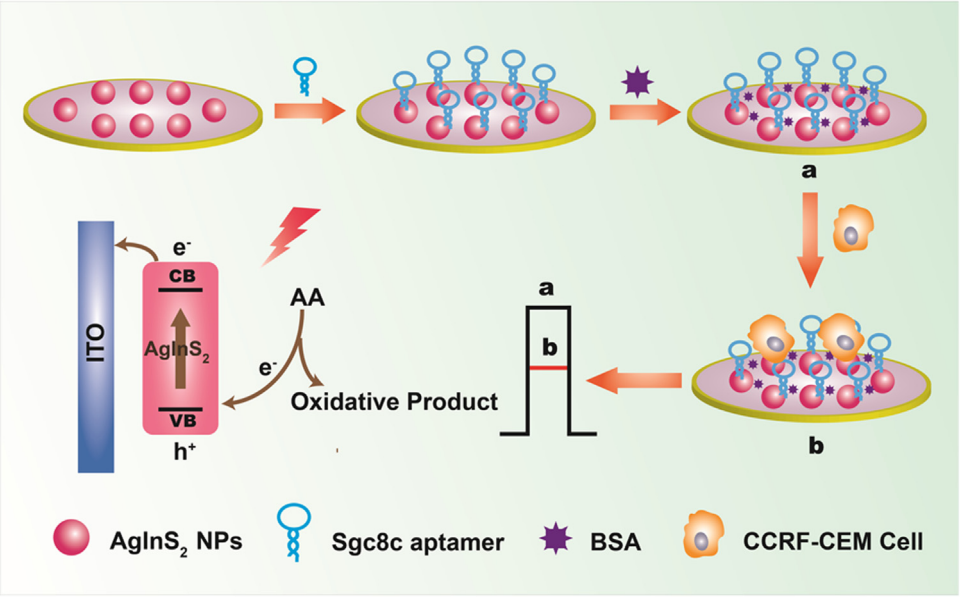

Scheme 1. Schematic illustration of red light-driven PEC biosensing platform for CCRF-CEM cells.

flow cytometric analysis was completed on BD Accuri C6 flow cytometer (BD Biosciences, San Jose, CA, USA). The (3-(4,5-dimethylthiazol-2-yl)-5-(3-carboxy- methoxyphenyl)-2-(4-sulfophenyl)-2H-tet-razolium (MTS) assay was measured at 490 nm by using a spectrophotometer (Thermo Scientific Multiskan GO, USA). The conventional three-electrode system was adopted to conduct all of experiments test at room temperature, which composed of that the modified ITO electrode acted as a working electrode, the platinum wire acted as an auxiliary electrode and the Ag/AgCl electrode acted as a reference electrode.

2.3. Synthesis of MPA-capped $AgInS_2$ nanoparticles

The MPA-capped $AgInS_2$ NPs were synthesized according to the previous literature (Jin et al., 2015; Tang et al., 2015), but the preparation method was slightly altered. Briefly, 0.5 mmoL of $AgNO_3$ and 1 mmol of indium (III) acetate were orderly dissolved in 4.5 mL of ethylene glycol. Subsequently, 610 μL of MPA was added dropwise into the above homogeneous solution. Then, the reaction mixture was stirred under a vacuum condition for 10 min, following heating to 150 °C under an argon atmosphere for 30 min. After cooling to room temperature, the samples were obtained by centrifugation and washing with ultrapure water for three times, then the final products were collected and dried at 60 °C in a vacuum drying oven. Finally, the 5 mg/mL of MPA-capped $AgInS_2$ nanoparticles aqueous suspension was obtained and stored at 4 °C.

2.4. Cell culture

The CCRF-CEM cells and Ramos cells were provided by Jiangsu Keygen Biotech Corp., Ltd. These suspension cells were cultured in RPMI-1640 medium containing 10% bovine serum (FBS) and incubated at 37 °C under 5% CO_2 in the cell incubator during development. The cells entering the logarithmic phase of growth were collected by centrifugation at 1000 rpm for 5 min and washed with 0.1 M phosphate buffer saline (PBS, pH 7.4) containing 136.75 mM NaCl, 2.28 mM KCl, 10.14 mM $Na_2HPO_4{\cdot}12H_2O$, and 1.76 mM KH_2PO_4, followed by, the collected cells were redispersed in PBS buffer saline containing 1 mM Ca^{2+} and 1 mM Mg^{2+} to reconstruct a homogeneous cell suspension. And then, the different levels of cells were obtained by using a cell-count board.

2.5. Cell viability

The conventional MTS assay as a colorimetric method was employed in examining the cytotoxicity of MPA-capped $AgInS_2$ NPs. Put simply, 50 μL of a density of 1×10^5 CCRF-CEM cells were inoculated in 96 well plate and treated with 50 μL various concentration of $AgInS_2$ NPs solution at 37 °C under 5% CO_2. After incubating for 24 h, 20 μL of MTS solution was added to these pores, and then they were further incubated for 4 h in the dark. The cell viability was evaluated based on the absorbance of samples at 490 nm with a microplate reader.

2.6. Construction of PEC cytosensing platform

Before the preparation of the work electrode, the ITO electrodes were cleaned by ultrasonic treatment process with acetone, 1 M NaOH/ethanol mixed solution (v/v, 1:1) and ultrapure water in turn according to the previous literature (Zhu et al., 2016), and then dried at 60 °C for further use. Firstly, 20 μL of 5 mg/mL homogeneous $AgInS_2$ NPs suspension was dropped onto the treated ITO electrode. After being dried at 37 °C, that electrode was covered with 20 μL of 10 mM EDC and 5 mM NHS mixed solution and incubated for 1 h at room temperature. Then, the electrode was rinsed with washing buffer. Subsequently, 20 μL of 1 μM amino-terminated sgc8c aptamer solution was modified on the surface of work electrode through the conjugation of the amine groups and the carboxyl groups of $AgInS_2$ NPs, and incubated at 4 °C for 12 h. After rinsing with washing buffer to remove the uncombined aptamer, the aptamer-functionalized $AgInS_2$ NPs/ITO electrode was obtained. To block nonspecific sites, the aptamer-functionalized electrode was further incubated with 20 μL of BSA (1%) for 1 h at room temperature, and then washed with ultrapure water to remove thoroughly excess BSA. Finally, the fabricated working electrode was stored at 4 °C for subsequent use.

2.7. PEC measurements

20 μL of CCRF-CEM cells with different concentrations were incubated on the surface of the work electrode at 4 °C for 1 h, after that, the PEC biosensor was rinsed with washing buffer to wash away the nonspecific adsorption of cells. Then, the biosensor was put into the Tris-HCl buffer saline (0.1 M, pH 7.4) containing 0.025 M AA, 0.1 M NaCl and 0.05 M KCl. The PEC detection system did not need deaeration with nitrogen. In addition, the PEC test process was maintained at an applied potential of 0.15 V under 630 nm light irradiation.

3. Results and discussion

3.1. Characterizations

The TEM image of the synthesized $AgInS_2$ NPs showed that the $AgInS_2$ NPs were well dispersed with an average diameter of 25 nm (Fig. 1A), which might be beneficial for photoinduced electron transfer. The $AgInS_2$ NPs suspension solution presented a redish-brown color and was sustained stabilization (Fig. 1A, inset). Optical properties of $AgInS_2$ NPs were displayed in UV–vis absorption and PL emission spectra. As shown in Fig. 1B, the UV–vis absorption spectrum of $AgInS_2$ NPs exhibited an acromion absorption peak at ~ 580 nm (curve a), which was identical with that of the previous report (Jin et al., 2015). Under 570 nm excitation, the PL spectrum of $AgInS_2$ NPs exhibited an intensive emission peak at 860 nm (curve b), which revealed that the $AgInS_2$ NPs was liable to generate photoexcited electron transport under long-wavelength light excitation (Ogawa et al., 2010). All the above results verified the $AgInS_2$ NPs were successfully prepared and implied that $AgInS_2$ NPs could be utilized for the construction of PEC biosensing platform.

Furthermore, to confirm the modification of carboxyl group on $AgInS_2$ NPs, the FTIR spectrum was performed (Fig. 1C). The O-H (3444 cm^{-1}), C=O (1720 cm^{-1}) and C-O (1251 cm^{-1}) stretching vibrations of the carboxyl group were observed, which indicated that the carboxyl group was successfully introduced on the surface of the $AgInS_2$ NPs. The introduction of carboxyl group might bring wonderful hydrophily (Fig. 1A, inset) and biocompatibility. The X-ray diffraction (XRD) pattern was used to verify the phase and structure of the obtained $AgInS_2$ NPs sample (Fig. 1D). As displayed, all of the diffraction peaks were ascribed to the orthorhombic $AgInS_2$ phase (JCPDS PDF 25-1328). The result of XRD pattern was in good agreement with those in the previous work (Jin et al., 2015).

Electrochemical impedance spectroscopy as a powerful tool was used to check surface modification process. With increasing modification of the ITO electrode, the changes in electron-transfer resistance (R_{et}) could be measured in 5 mM $K_3Fe(CN)_6/K_4Fe(CN)_6$ (v/v, 1:1) solution containing 0.1 M KCl (Li et al., 2016). As displayed in Fig. 2A, when $AgInS_2$ NPs were modified on the bare ITO electrode, a lager semicircle diameter was obtained (curve b), compared with that of bare ITO electrode (curve a). The above changes suggested its success in the fabrication of $AgInS_2$/ITO electrode. Subsequently, after the aptamer was immobilized on the electrode via the formation of amide bond between aptamer and $AgInS_2$ NPs, the value of R_{et} exhibited an apparent increase (curve c), which was owing to the poor conductivity and the electronegativity of single strand DNA (Liu et al., 2016) that impeded the access of redox probe to the surface of the electrode. Next,

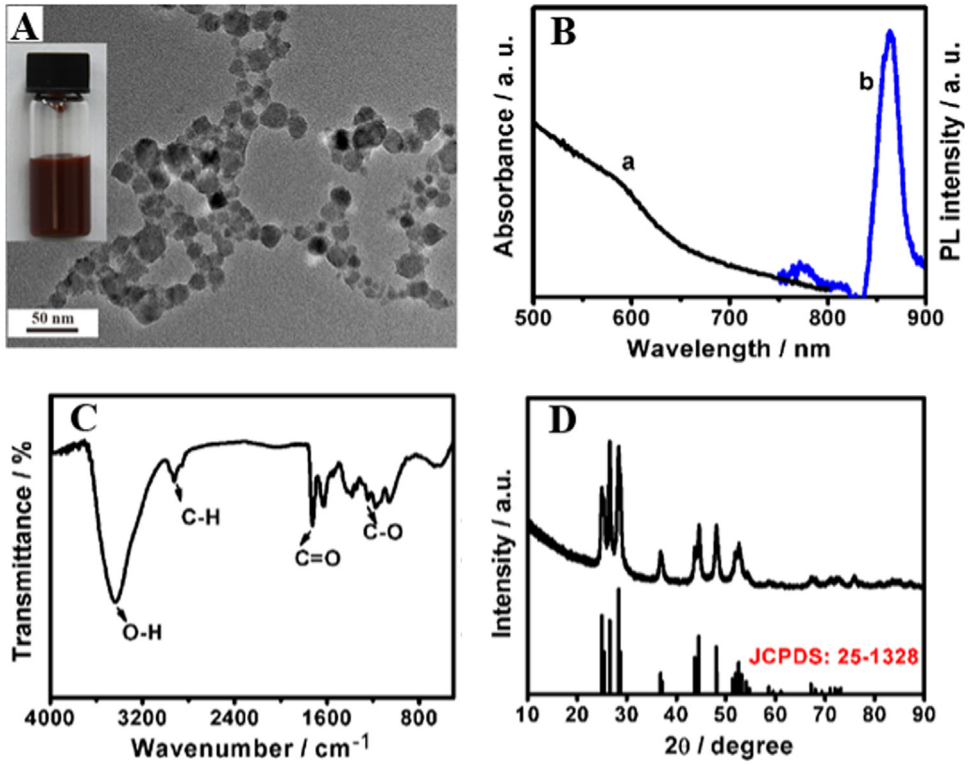

Fig. 1. (A) TEM image of the as-synthesized $AgInS_2$ Nanoparticles. (B) UV–vis (a) and PL (b) spectra of $AgInS_2$ NPs. (C) FT-IR spectrum and (D) XRD pattern of $AgInS_2$ NPs.

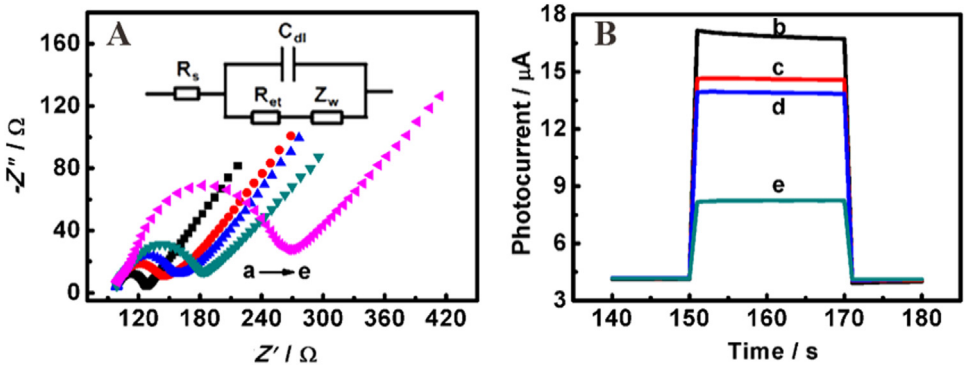

Fig. 2. (A) Nyquist diagrams and (B) PEC responses of bare ITO (a), $AgInS_2$ NPs/ITO (b), aptamer/$AgInS_2$ NPs/ITO (c), BSA/aptamer/$AgInS_2$ NPs/ITO (d) and (6000 cells/mL) cells/BSA/aptamer/$AgInS_2$ NPs/ITO (e) electrodes.

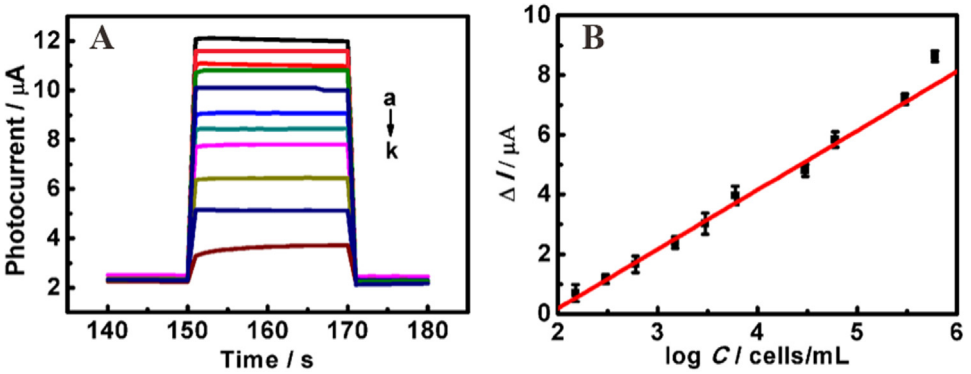

Fig. 3. (A) Photocurrent response of the PEC cytosensor toward CCRF-CEM cells with different concentrations (a-k) 0, 1.5×10^2, 3×10^2, 6×10^2, 1.5×10^3, 3×10^3, 6×10^3, 3×10^4, 6×10^4, 3×10^5, 6×10^5 cells/mL. (B) The linear calibration curve.

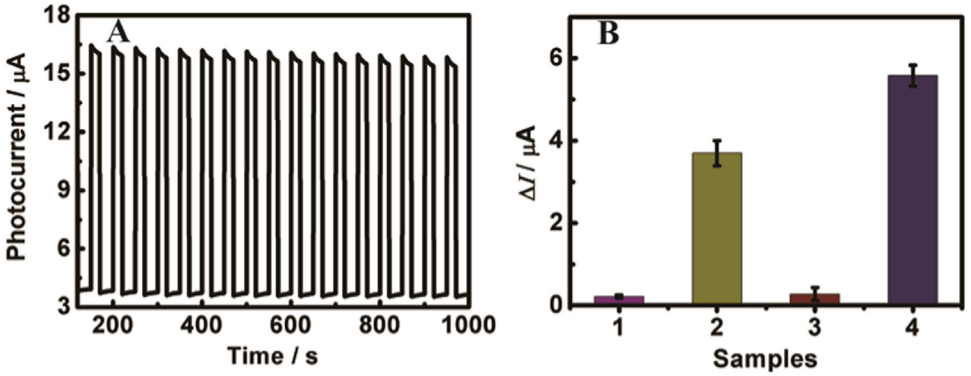

Fig. 4. (A) Time-based photocurrent response of the $AgInS_2$ NPs-modified electrode. (B) PEC response of the cytosensor toward 6×10^3 cells/mL Ramos cells (sample 1), 6×10^3 cells/mL Ramos cells $+ 6 \times 10^3$ cells/mL CCRF-CEM cells (sample 2), 6×10^4 cells/mL Ramos cells (sample 3) and 6×10^4 cells/mL Ramos cells $+ 6 \times 10^4$ cells/mL CCRF-CEM cells (sample 4).

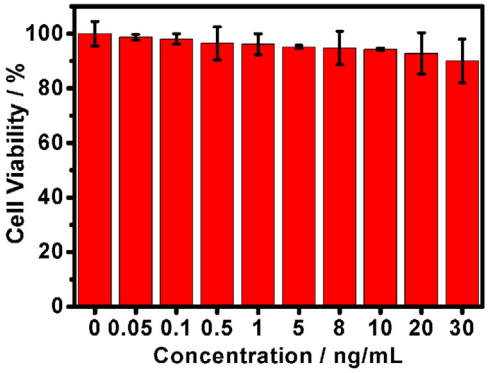

Fig. 5. Growth inhibition results for CCRF-CEM cells treated with $AgInS_2$ NPs with concentrations of 0–30 ng/mL under 490 nm irradiation.

the blocking of BSA further caused the enhancement of R_{et} value (curve d), owing to the steric hindrance of protein that hindered the transfer of redox probe. Lastly, R_{et} promoted significantly after incubation with CCRF-CEM cells (curve e). The insulated cells formed an insulating layer on the electrode surface, which generated the remarkable steric hindrance that dramatically hindered the transfer of redox probe to the electrode surface. In conclusion, the changes of electron-transfer resistance with the successive assembly verified that the PEC cytosensing platform was successfully developed.

3.2. PEC behaviors of the modified electrodes and feasibility of the proposed strategy

The feasibility of the designed strategy was illustrated by examining the variation of the photocurrent intensity via layer-by-layer assembly of the electrode surface (Fig. 2B). The $AgInS_2$ NPs-modified electrode displayed an intensive and stable anodic photocurrent (~ 16.87 μA) in Tris-HCl buffer saline (0.1 M, pH 7.4) containing 0.025 M AA under 630 nm irradiation at 0.15 V (curve b), owing to the effective separation of electron-hole pairs in $AgInS_2$ NPs. The narrow band gap of $AgInS_2$ NPs which had an excellent absorption in red light region (Foda et al., 2014) could be easily excited under visible light irradiation, leading to generation of the electron-hole pairs. The photo-generated holes located at valence band (VB) were scavenged by AA, which inhibited the recombination of electron-hole pairs (Scheme 1). Meanwhile, the electrons of conduction band (CB) transferred to the ITO electrode, leading to a stable anodic photocurrent. After immobilizing with the sgc8c aptamer and blocking with BSA, the photocurrent values declined to 14.63 μA (curve c) and 13.91 μA (curve d), respectively. The steric hindrance of the modifiers hindered the electron donor to the VB of $AgInS_2$ NPs, leading to the decrease of photocurrent intensity. While CCRF-CEM cells were bond to the aptamer, the photocurrent intensity dramatically decreased to 8.25 μA (curve e), which was 59% of that without CCRF-CEM cells (curve d). The wonderful decline of photocurrent intensity might be ascribed to two aspects. For one thing, the surface of CCRF-CEM cells possessed hydrophobicity which blocked the hydrophilic AA to the surface of $AgInS_2$ NPs. For another, the huge steric hindrance of CCRF-CEM cells impeded the photoinduced electron and charge transfer. The significant difference of PEC response (5.66 μA) in the presence (curve e) and absence (curve d) of CCRF-CEM cells advantageously provided ultrahigh sensitivity for PEC detection of CCRF-CEM cells, validating the feasibility of the proposed strategy.

3.3. Optimization of the detection conditions

To achieve satisfactory PEC biosensing platform, several important experiment parameters were optimized such as the concentrations of AA and $AgInS_2$ NPs, and the applied voltage. $AgInS_2$ NPs as photoelectrochemically active species are a core part in PEC output signal, therefore its level directly affects the photocurrent response. The relationship was investigated specifically in Fig. S1A. Under 630 nm excitation at 0.15 V, the photocurrent intensity gradually enhanced by increasing $AgInS_2$ NPs concentration from 3 to 5 mg/mL and then sharply declined over 5 mg/mL. The excess $AgInS_2$ NPs might influence photoinduced electron and charge transfer to the electrode surface (Dai et al., 2016). Thus, 5 mg/mL as an optimized concentration was selected for PEC measurement.

The bias voltage is a vital parameter, which affects PEC performance. As shown in Fig. S1B, the photocurrent intensity reached a maximum value at 0.15 V and it leveled off ranging from 0.15 to 0.20 V under 630 nm irradiation. Then the PEC response dramatically fell once beyond 0.20 V. Hence, 0.15 V was chosen as the applied potential for PEC detection.

Ascorbic acid acts as an electron donor in order to gain a steady and intensive enough photocurrent signal. Consequently, the concentration of AA as a key parameter was investigated (Fig. S1C). The photocurrent intensity increased with the rise of AA concentration from 0.0125 to 0.025 M, while its changes were slight after increasing AA concentration from 0.025 to 0.15 M. Such phenomenon indicated that 0.025 M AA was enough to occupy the photoinduced holes located at the VB of $AgInS_2$ NPs, implying a formation of saturated electron donor in the photoinduced holes. As a result, 0.025 M was the optimal concentration for PEC determination.

As mentioned above, the photocurrent was influenced by the immobilization of aptamer on the electrode surface which could effectively capture CCRF-CEM cells in the PEC detection system. Generally speaking, the analytical performance of the developed PEC cytosensor can be improved by regulating the concentration of the sgc8c aptamer (Pang et al., 2018) and incubation time of CCRF-CEM cells. As shown in Fig. S2A, the photocurrent intensity sharply declined after the concentration of aptamer was more than 1 μM. The aptamer with excessive concentration owned huge steric hindrance, which might impede the photoinduced electron and charge transfer. Therefore, 1 μM was chosen as the optimal concentration. As seen from Fig. S2B, the PEC response

decreased with increasing the incubation time from 15 to 60 min, and then it remained relatively stable after 60 min, indicating the equilibrium of saturated reaction. Consequently, an incubation time of 60 min was selected for the cytosensing system.

3.4. PEC cytosensing

Under the optimum conditions (Fig. S1 and Fig. S2 in the Supplementary information), the different concentrations of CCRF-CEM cells were detected by the designed PEC strategy, and the corresponding photocurrent responses were displayed in Fig. 3A. The photocurrent intensity decreased with the rise of cells suspension concentration. It was found that its variation had a good linear response with the logarithm of CCRF-CEM cells concentration in the range of 1.5×10^2 to 3×10^5 cells/mL (Fig. 3B). The linear equation was represented as ΔI (μA) = 1.986 lg C −3.791 (cells/mL) with its correlation coefficient of 0.995 ($\Delta I = I - I_0$, where I represented the photocurrent intensity after incubating target cells at different concentrations and I_0 was the photocurrent intensity before incubating target cells). The detection limit was estimated to be 16 cells/mL at 3σ (where σ was the relative standard deviation of eleven parallel measurements when CCRF-CEM cell concentration was zero), which was much lower than most reported methods (Table S2 in the Supplementary information), indicating an ultrahigh sensitivity of the proposed PEC biosensing strategy for tumor cells under red light excitation. Besides, the Cy3 labeled sgc8c aptamer binding conjugates with different concentration of CCRF-CEM cells were detected by flow cytometry assay (Fig S3 and Fig S4 in the Supplementary information). Comparing with the assay results between the flow cytometry and the proposed biosensor, an acceptable agreement with relative error of less than 8.79% was displayed (Table S1 in the Supplementary information), indicating the satisfactory accuracy of the proposed PEC biosensor.

3.5. The stability and selectivity of the cytosensor

The operation stability is the main factor limiting the further application of the PEC biosensor, which was evaluated via the variation degree of photocurrent. After 17 on-off cycles of PEC test, the photocurrent of the $AgInS_2$ NPs-modified electrode almost had no obvious change and retained 96.8% of its initial photocurrent response (Fig. 4A). Based on the good operation stability of $AgInS_2$ NPs-modified electrode, it could be applied to the fabrication of PEC cytosensing platform as a photoelectrochemically active species. The selectivity of the developed PEC cytosensor for CCRF-CEM cells was explored by the comparison of the photocurrent response toward Ramos cells with that of their mixture (Fig. 4B). Under the same test conditions, the photocurrent of sample 1 and sample 3 had no obvious change, compared with the appreciable photocurrent drop of sample 2 and sample 4. The result demonstrated that the developed PEC cytosensor had good selectivity for CCRF-CEM cells assay.

3.6. Cell viability investigation

The cytotoxicity of the proposed PEC biosensing strategy was illustrated by MTS assay. Growth inhibition results for CCRF-CEM cells treated with $AgInS_2$ NPs at different concentrations under 490 nm irradiation were exhibited in Fig. 5. After 24 h incubation, the cell viability was 95.21%, 94.79% and 94.34% at concentration of 10, 20 and 30 ng/mL, respectively, suggesting a negligible cytotoxicity. Therefore, the designed PEC biosensing method displayed high viability and satisfactory biocompatibility for cell assay.

4. Conclusions

In this work, a novel PEC biosensing strategy was proposed for ultrasensitive and scatheless assay of cell by the specific binding of the sgc8c aptamer modified $AgInS_2$ NPs and protein tyrosine kinase-7 on living CCRF-CEM cells surface under a red light excitation. Ternary MPA-capped $AgInS_2$ NPs as PEC biosensing substrate material with excellent hydrophily and biocompatibility exhibited a steady and intensive photocurrent response, which much improved the sensitivity of PEC detection. Herein, using CCRF-CEM cell as a model analyte, an ultrasensitive PEC biosensor for scatheless assay of cells at the bias voltage of 0.15 V under 630 nm irradiation was developed based on the dramatical decline of photocurrent intensity after capturing CCRF-CEM cells. The changes of electron-transfer resistance with the successive assembly confirmed the successful construction of the PEC cytosensor. The proposed cytosensor displayed satisfactory analytical performance towards CCRF-CEM cells, such as wide linear response range, low detection limit, high specificity and negligible cytotoxicity. More importantly, this work not only extends the application of ternary I−III−VI semiconductor material in PEC sensing device, but also serves as an impetus for promoting the development of early clinical diagnoses of cancer. Owing to the limitation of miniaturizing the working electrode, the biggest challenge will be in situ and on-line monitoring for the level of tumor cells in vivo by using the proposed PEC biosensing strategy. Therefore, this designed PEC biosensing method has significant distance from cell analysis in vitro to living diagnosis in vivo.

Acknowledgements

This work was supported by the National Natural Science Foundation of China for the project (21625502 and 21475062) and Natural Science Foundation of Jiangsu Province of China (BK20171271). We appreciate the financial support from the Priority Academic Program Development of Jiangsu Higher Education Institutions.

Appendix A. Supporting information

Supplementary data associated with this article can be found in the online version at doi:10.1016/j.bios.2018.09.096

References

Cao, J., Zhao, X.P., Younis, M.R., Li, Z.Q., Xia, X.H., Wang, C., 2017. Anal. Chem. 89, 10957–10964.
Dai, H., Zhang, S.P., Hong, Z.S., Lin, Y.Y., 2016. Anal. Chem. 88, 9532–9538.
Dai, M.L., Ogawa, S., Kameyama, T., Okazaki, K., Kudo, A., Kuwabata, S., Tsuboi, Y., Torimoto, T., 2012. J. Mater. Chem. 22, 12851–12858.
Fan, G.C., Zhu, H., Shen, Q.M., Han, L., Zhao, M., Zhang, J.R., Zhu, J.J., 2015. Chem. Commun. 51, 7023–7026.
Feng, J.H., Li, Y.Y., Gao, Z.Q., Lv, H., Zhang, X.B., Fan, D.W., Wei, Q., 2018. Biosens. Bioelectron. 99, 14–20.
Foda, M.F., Huang, L., Shao, F., Han, H.Y., 2014. ACS Appl. Mater. Interfaces 6, 2011–2017.
Gai, P.P., Ji, Y.S., Wang, W.J., Song, R.B., Zhu, C., Chen, Y., Zhang, J.R., Zhu, J.J., 2016. Nano Energy 19, 541–549.
Gromova, M., Lefrancois, A., Vaure, L., Agnese, F., Aldakov, D., Maurice, A., Djurado, D., Lebrun, C., Geyer, Ad, Schulli, T.U., Pouget, S., Reiss, P., 2017. J. Am. Chem. Soc. 139, 15748–15759.
Halder, G., Bhattacharyya, S., 2017. J. Mater. Chem. A 5, 11746–11755.
Hamanaka, Y., Ogawa, T., Tsuzuki, M., 2011. J. Phys. Chem. C 115, 1786–1792.
Hong, S.P., Park, H.K., Oh, J.H., Yang, H., Do, Y.R., 2012. J. Mater. Chem. 22, 18939–18949.
Hu, T., Zheng, Y.N., Li, M.J., Liang, W.B., Chai, Y.Q., Yuan, R., 2018. Anal. Chem. 90, 6096–6101.
Jara, D.H., Yoon, S.J., Stamplecoskie, K.G., Kamat, P.V., 2014. Chem. Mater. 26, 7221–7228.
Jin, H., Gui, R.J., Wang, Z.H., Xia, J.F., Yang, M., Zhang, F.F., 2015. RSC Adv. 5, 68287–68292.
Kameyama, T., Koyama, S., Yamamoto, T., Kuwabata, S., Torimoto, T., 2018. J. Phys. Chem. C 122, 13705–13715.
Kobosko, S.M., Jara, D.H., Kamat, P.V., 2017. ACS Appl. Mater. Interfaces 9, 33379–33388.
Li, J., Tu, W.W., Li, H.B., Bao, J.C., Dai, Z.H., 2014. Chem. Commun. 50, 2108–2110.
Li, R.Y., Yan, R., Bao, J.C., Tu, W.W., Dai, Z.H., 2016. Chem. Commun. 52, 11799–11802.
Li, X., Zhu, L.S., Zhou, Y.L., Yin, H.S., Ai, S.Y., 2017. Anal. Chem. 89, 2369–2376.

Li, Y.J., Ma, M.J., Zhu, J.J., 2012. Anal. Chem. 84, 10492–10499.
Li, Z.Z., Xin, Y.M., Zhang, Z.H., 2015. Anal. Chem. 87, 10491–10497.
Ogawa, T., Kuzuya, T., Hamanaka, Y., Sumiyama, K., 2010. J. Mater. Chem. 20, 2226–2231.
Pang, X.H., Cui, C., Su, M.H., Wang, Y.G., Wei, Q., Tan, W.H., 2018. Nano Energy 46, 101–109.
Qiu, Z.L., Shu, J., Tang, D.P., 2018. Anal. Chem. 90, 1021–1028.
Sandroni, M., Wegner, K.D., Aldakov, D., Reiss, P., 2017. ACS Energy Lett. 2, 1076–1088.
Shamirian, A., Appelbe, O., Zhang, Q.B., Ganesh, B., Kron, S.J., Snee, P.T., 2015. J. Mater. Chem. B 3, 8188–8196.
Shen, S.L., Wang, Q.B., 2013. Chem. Mater. 25, 1166–1178.
Subramaniam, P., Lee, S.J., Shah, S., Patel, S., Starovoytov, V., Lee, K.B., 2012. Adv. Mater. 24, 4014–4019.
Shangguan, D.H., Tang, Z.W., Mallikaratchy, P., Xiao, Z.Y., Tan, W.H., 2007. ChemBioChem 8, 603–606.
Tang, J., Zhang, Y., Kong, B., Wang, Y., Da, P.M., Li, J., Elzatahry, A.A., Zhao, D.Y., Gong, X.G., Zheng, G.F., 2014. Nano Lett. 14, 2702–2708.
Tang, R., Xue, J.P., Xu, B.G., Shen, D.W., Sudlow, G.P., Achilefu, S., 2015. ACS Nano 9, 220–230.
Tu, W.W., Wang, Z.Y., Dai, Z.H., 2018. TrAC-Trends Anal. Chem. 105, 470–483.
Wang, H.Y., Qi, C.L., He, W.H., Wang, M.H., Jiang, W.J., Yin, H.S., Ai, S.Y., 2018. Biosens. Bioelectron. 99, 281–288.
Wang, L., Kang, X., Pan, D., 2017. Inorg. Chem. 56, 6122–6130.
Wen, G.M., Ju, H.X., 2016. Anal. Chem. 88, 8339–8345.
Xiong, W.W., Yang, G.H., Wu, X.C., Zhu, J.J., 2013. J. Mater. Chem. B 1, 4160–4165.
Yan, Z.Y., Wang, Z.H., Miao, Z., Liu, Y., 2016. Anal. Chem. 88, 922–929.
Yarema, O., Yarema, M., Wood, V., 2018. Chem. Mater. 30, 1446–1461.
Zang, Y., Lei, J.P., Ling, P.H., Ju, H.X., 2015. Anal. Chem. 87, 5430–5436.
Zhao, W.W., Xu, J.J., Chen, H.Y., 2015. Chem. Soc. Rev. 44, 729–741.
Zhao, W.W., Xu, J.J., Chen, H.Y., 2017. Biosens. Bioelectron. 92, 294–304.
Zhong, H.Z., Bai, Z.L., Zou, B.S., 2012. J. Phys. Chem. Lett. 3, 3167–3175.
Zhu, H., Fan, G.C., Abdel-Halim, E.S., Zhang, J.R., Zhu, J.J., 2016. Biosens. Bioelectron. 77, 339–346.